

Contents lists available at ScienceDirect

Polymer

journal homepage: www.elsevier.com/locate/polymer





Hybrid silver nanoparticles with controlled morphology as efficient substrates for surface-enhanced Raman scattering

Krzysztof Jerczynski ^a, Julita Muszynska ^b, Gokhan Demirci ^{a,c}, Onur Cetinkaya ^{b,d}, Paulina Filipczak ^b, Grzegorz Nowaczyk ^e, Jaroslaw Grobelny ^f, Krzysztof Matyjaszewski ^{b,g}, Marcin Kozanecki ^{b,**}, Joanna Pietrasik ^{a,*}

- a Institute of Polymer and Dye Technology, Lodz University of Technology, Faculty of Chemistry, Stefanowskiego 16, 90-537, Lodz, Poland
- b Department of Molecular Physics, Lodz University of Technology, Faculty of Chemistry, Zeromskiego 116, 90-543, Lodz, Poland
- ^c Department of Polymer and Biomaterials Science, Faculty of Chemical Technology and Engineering, West Pomeranian University of Technology in Szczecin, Al. Piastów 45, 70-311, Szczecin, Poland
- d Department of Pharmaceutical Chemistry, Faculty of Pharmacy, Kocaeli Health and Technology University, 41275, Kocaeli, Turkey
- e NanoBioMedical Centre, Adam Mickiewicz University in Poznan, Wszechnicy Piastowskiei 3, 61-614, Poznan, Poland
- f Department of Materials Technology and Chemistry, Faculty of Chemistry, University of Lodz, Pomorska 163, 90-236, Lodz, Poland
- g Department of Chemistry, Carnegie Mellon University, 4400 Fifth Avenue, Pittsburgh, PA, 15213, United States

ARTICLE INFO

Keywords: Star-like polymers Unimolecular templates Silver nanoparticles Surface-enhanced Raman spectroscopy

ABSTRACT

This work reports on the efficient performance of hybrids particles with silver nanoparticles (AgNPs) distributed within single polymer molecules with star-like topology as Surface Enhanced Raman Scattering (SERS) supports. First, the library of the star-like polymers with poly (acrylic acid)-block-polystyrene (PAA-b-PS) arms was obtained via atom transfer radical polymerization (ATRP) using a "core-first" approach. Then, hybrid silver nanoparticles were synthesized in a controlled way within the prepared single molecules playing the role of molecular templates for AgNPs. Finally, the hybrid particles were tested as novel substrates for SERS using crystal violet as an analyte. Synthesized star-like templates had varied number of arms within the single star, the order of PAA and PS blocks, their degree of polymerization, and the molar ratio of the carboxylic groups of PAA block to the nanoparticles' precursor. Additionally, the minimum analyte concentration required for SERS was determined. The number of arms within a polymer template plays a crucial role in the synthesis of silver nanoparticles and observed SERS effect. Prepared substrates were stable for long time and allowed the detection of the analytes on the nanomolar level.

1. Introduction

Surface Enhanced Raman Scattering (SERS) technique is a unique analytical method that allows shifting the detection threshold down to a very small concentration (to nano or even picomolar range) of analyte i. e., mainly different organic molecules including biologically active ones [1,2]. Thus, a lot of effort is devoted to developing stable, effective, and universal SERS supports [2,3]. SERS phenomenon occurs due to the amplification of scattered light by localized surface plasmon resonance (LSPR). Through interactions between light and metal nanoparticles, surface plasmons are generated and their collective oscillations lead to significant amplification of the signal. Two mechanisms are believed to

contribute to the SERS phenomenon: Chemical Mechanism (CE) and Electromagnetic Mechanism (EM) [4–6]. The first is based on electron transfer between analyte and nanoparticles and brings a slight enhancement up to three orders of magnitude. The latter mechanism consists of obtaining the resonance effect between the electrons of the analyte molecule and the surface plasmons of nanoparticles (NPs), resulting in a signal amplification even to 10¹⁵ [4]. Therefore, there are certain factors affecting the Raman signal enhancement, the most important are: the size and shape of nanoparticles, distance between them, type of metal, chemical structure, affinity to NPs of an analyte, power of the exciting beam, exposure time, and Raman cross-section of an analyte. The most effective SERS have been observed for noble metal

E-mail addresses: marcin.kozanecki@p.lodz.pl (M. Kozanecki), joanna.pietrasik@p.lodz.pl (J. Pietrasik).

^{*} Corresponding author.

^{**} Corresponding author.

nanoparticles (Au, Ag), and the most desirable are those with spiked parts, for example, star-like or flower-like forms, due to the enormous electromagnetic field accumulated in these regions. The metal nanoparticles of such complex shapes have also high surface energy and the tendency for agglomeration and/or aggregation, so the problem of their stability is the next important challenge. Furthermore, the distance between the metal NPs should be also precisely controlled in a range from a few to a dozen or so nanometers (that distance is necessary to give a space for analyte penetration) to reach a high SERS effect [7,8].

High control of nanoparticles' morphology can be achieved by using different types of polymer templates for nanoparticle synthesis. In general, linear polymers cannot be used as effective templates because they do not provide sufficient stability of nanoparticles during the synthesis [9]. However, under certain conditions, linear block copolymers with proper chemical composition can self-organize into micelles which are stable structures within selected environments and were successfully used as templates for the synthesis of various nanoparticles [10-13]. Polymer micelles can be also obtained via polymerization-induced self-assembly (PISA) and further applied as templates for the synthesis of nanoparticles [14,15]. Another approach is to use more complex molecules, such as nanogels [16,17], star-like or brush-like polymers [18] as templates which can also effectively prevent against aggregation of metal NPs and enhance their stability, provide solubility in selected solvents, and improve distribution in polymer matrixes [19]. The main advantage of such a system is that the size and shape of the nanoparticles may be predetermined by the degree of polymerization and chemical composition of the polymer templates. A variety of nanoparticles with varied properties (optical, magnetic, electric, semiconducting, catalytic), morphologies (filled, hollow, and core-shell spheres or rods), and applications (nanofillers for polymer matrixes, additives to dielectric layers in organic field effect transistors) were synthesized [9,19-24].

In our previous works, poly(acrylic acid)-block-polystyrene (PAA-b-PS) and poly(acrylic acid-stat-acrylamide)-block-polystyrene (P (AA-stat-Am)-b-PS) micelles obtained via PISA were used as effective templates for Ag nanoparticles. Obtained materials were successfully used as substrates for SERS [14,15]. Due to the size of the templates, it was difficult to control the number and morphology of AgNPs generated within a single polymer micelle. Herein, single macromolecules with star-like architecture were used as unimolecular polymer templates for the synthesis of hybrid silver nanoparticles. First, initiators containing 3, 17, 50, and 280 initiation sites were prepared from 1,1,1-tris(4-2-bromoisobutyryloxy)phenyl)ethane (TBPE) and poly (2-bromoisobutyrvloxyethyl methacrylate) (PBiBEM), respectively. Then, PAA-b-PS arms were synthesized using the "core-first" and "grafting-from" approach via atom transfer radical polymerization (ATRP) [25-29]. Next, the prepared polymer templates were used for the in-situ synthesis of Ag nanoparticles, which were finally tested as potential substrates for SERS spectroscopy. Systematic studies were carried out to check how the topology of the polymer template influences the synthesis of AgNPs and SERS effect.

2. Experimental part

2.1. Materials

Tert-butyl acrylate (*t*BA, 99%) received from Alfa Aesar and styrene (S, \geq 99%) received from Sigma Aldrich were purified by distillation under reduced pressure. 2-(Trimethylsilyloxy)ethyl methacrylate (HEMA-TMS, 96%) received from Sigma Aldrich was purified by passing through the basic aluminum oxide. 2,2'-Azobis(isobutyronitrile) (AIBN) received from Sigma Aldrich was purified by recrystallization. Copper (I) chloride (CuCl₂, \geq 99%), copper (II) chloride (CuCl₂, \geq 99.999%), copper (I) bromide (CuBr₂, \geq 99.999%), 4,4'-dinonyl-2,2'-dipyridyl (dNbpy, \geq 97%), *N,N,N',N'',N''*-pentamethyldiethylenetriamine (PMDETA, \geq 99%), ethyl α-bromoisobutyrate (EBiB, \geq 98%), α-bromoisobutyryl bromide (BIBB, \geq 98%), potassium

fluoride (KF, \geq 99%), 2,6-di-*tert*-butylphenol (DTBP, 99%), tetrabutylammonium fluoride (TBAF, 1.0 M in THF), silver nitrate (AgNO₃, \geq 99.8%), sodium borohydride (NaBH₄, \geq 99%), trifluoroacetic acid (TFA, 99%), 1,1,1-tris(4-hydroxyphenyl)ethane (THPE, 99%), triethylamine (TEA, \geq 99.5% (GC)), dimethyl sulfoxide (DMSO, anhydrous, \geq 99.9%) were used as received from Sigma Aldrich. Magnesium sulfate (98.0%) was used as received from Fluorochem. Solvents: dichloromethane (DCM, 99.8%), *N*,*N*-dimethylformamide (DMF, 99.8%), ethyl acetate (99.5%), methanol (MeOH, 99%), *n*-hexane (99%), tetrahydrofuran (THF, 99.8%) were provided by Avantor Performance Materials Poland. Anisole (99%) was provided by Acros Organics.

2.2. Synthesis

All polymer templates used within these studies were obtained according to the general procedure described below for 3-arm star polymer. Molar ratios for all syntheses are presented in Table S1 (see Supplementary Information).

2.2.1. Synthesis of 1,1,1-tris(4-(2-bromoisobutyryloxy)phenyl)ethane initiator (TBPF)

Synthesis of 1,1,1-tris(4-(2-bromoisobutyryloxy)phenyl)ethane (TBPE) was carried out according to an already published procedure, molar ratios were THPE:BIBB:TEA = 1:3.94:6 [30].

2.2.2. Synthesis of TBPE-(PtBA₁₃₆)₃ stars

TBPE (0.0286 g, 0.114 mmol) obtained in the previous step, CuBr $_2$ (0.0013 g, 0.006 mmol), and CuBr (0.0074 g, 0.051 mmol) were weighted into a Schlenk flask and degassed by argon purging for 45 min. Then, degassed anisole (1.11 mL, 10% v/v), tBA (10.00 mL, 68.238 mmol), and PMDETA (12 μL , 0.057 mmol) were added. The flask was placed in a preheated oil bath at 70 °C while stirring. After the monomer conversion reached 22.7% (determined by $^1 H$ NMR), the reaction mixture was cooled to RT, diluted with dichloromethane (DCM), and passed through a neutral alumina column. The solvent and remaining monomer were removed by dialysis in MeOH/THF mixture (1/1 v/v) using Regenerated Cellulose Dialysis Membrane ZelluTransRoth MWCO 3500. A white solid product was obtained after drying in a vacuum oven at 30 °C and 10 mbar.

2.2.3. Synthesis of TBPE-(PtBA $_{136}$ -b-PS $_{29}$) $_3$ stars

TBPE-($PtBA_{136}$)₃ (0.5000 g, 0.028 mmol) obtained in the previous step, CuBr₂ (0.0006 g, 0.003 mmol), and CuBr (0.0037 g, 0.025 mmol) were weighted into a Schlenk flask and degassed by argon purging for 45 min. Then, degassed anisole (0.50 mL, 22% v/v), S (1.80 mL, 12.725 mmol), and PMDETA (6 μ L, 0.031 mmol) were added. The flask was placed in a preheated oil bath at 60 °C while stirring. After the monomer conversion reached 6.5% (determined by 1 H NMR), the reaction mixture was cooled to RT, diluted with DCM, passed through a neutral alumina column, concentrated, re-precipitated three times in methanol, and dried in a vacuum oven at 30 °C and 10 mbar.

2.2.4. Hydrolysis of TBPE-(PtBA₁₃₆-b-PS₂₉)₃ stars

TBPE-($PtBA_{136}$ -b- PS_{29}) $_3$ star polymer (0.0500 g, 0.00034 mmol of AA units) obtained in the previous step was dissolved in 3 mL of DCM. Then trifluoroacetic acid (127 μ L, 0.0017 mmol) was added dropwise. The reaction was carried out at RT for 48 h. Later, the reaction mixture was precipitated once in n-hexane. A white solid product was obtained after drying in a vacuum oven at 30 $^{\circ}$ C and 10 mbar.

2.2.5. Synthesis of silver nanoparticles

Silver nanoparticles were obtained according to the general procedure. Templates were dissolved in DMSO to prepare solutions with a concentration of 1 mg/mL. Then, three varied amounts of silver precursor solutions were added (1 mg/mL of AgNO $_3$ in DMSO; -COO $^\prime$ Ag $^+$ = 2:1, 1:1, 1:2) and reaction mixtures were stirred for 1 h at RT to allow

the incorporation of the precursor within the templates. Next, a reducing agent solution (0.1 mg/mL of NaBH₄ in DMSO; NaBH₄/Ag $^+=1:1$) was added dropwise. After 15 min of stirring, vials were closed and stored in the dark for 48 h.

2.2.6. Synthesis of P(HEMA-TMS)₁₇ stars [25,31,32]

dNbpy (0.0900 g, 0.220 mmol), CuCl $_2$ (0.0069 g, 0.051 mmol), and CuCl (0.0058 g, 0.059 mmol) were weighted into a Schlenk flask and degassed by argon purging for 45 min. Then degassed anisole (0.45 mL, 10% v/v), HEMA-TMS (4.00 mL, 18.347 mmol), and EBiB (27 μ L, 0.183 mmol) were added. The flask was placed in a preheated oil bath at 60 °C while stirring. After the monomer conversion reached 17% (determined by 1 H NMR), the reaction mixture was cooled to RT, diluted with DCM, passed through a neutral alumina column, concentrated, and used in the next step.

2.2.7. Synthesis of PBiBEM₁₇ stars [25,31,32]

KF (1.8122 g, 31.19 mmol) and DTBP (0.4921 g, 2.39 mmol) were weighted into a three-neck flask equipped with a condenser. Then, P (HEMA-TMS) $_{17}$ (3.7120 g, 18.35 mmol), and dry THF (50 mL, 93% v/v) were added, and the reaction mixture was degassed by argon for 45 min. The flask was cooled down in an ice bath, next TBAF (0.18 mL, 1.0 M in THF, 0.18 mmol), and BIBB (2.72 mL, 22.02 mmol) were added dropwise in 20 min. The reaction mixture reached RT and it was carried out for 24 h. Later, solids were filtered off and the polymer was precipitated in a methanol/water solution (7/3 v/v). The solids were dissolved in DCM, passed through a basic alumina column, concentrated, reprecipitated three times in n-hexane, and dried in a vacuum oven at 30 °C and 10 mbar.

Backbones with DP = 50 and 280 were prepared using analogous conditions; first, the synthesis of PtBA, next the extension with PS, and the hydrolysis of PtBA units were carried out according to conditions presented for 3-arm star polymers and molar ratios given in Table S1.

2.3. Characterization

2.3.1. Proton nuclear magnetic resonance characterization (¹H NMR)

 1 H NMR was used to calculate the monomer conversion and degree of polymerization (DP) of the synthesized polymers. The 1 H NMR spectra were recorded using a Bruker Avance II Plus 16.4 T spectrometer (Bruker BioSpin, Germany) operated at 250 and 700 MHz for 1 H experiments. Samples were prepared by dissolving a polymer in DMSO- d_6 or CDCl $_3$.

2.3.2. Gel permeation chromatography characterization (GPC)

GPC was used to determine the weight average and number average molecular weights of the synthesized polymers and their dispersity (\mathcal{D}). The GPC measurements were performed with a Wyatt (Wyatt, Dernbach, Germany) instrument equipped with two Perfect Separation Solutions (PSS) columns and one guard column (GRAM Linear (10 μ m, $M_n=800-1~000~000~g/mol$), differential refractometer (RI) and multi angle light scattering (MALS) detectors. The measurements were performed in DMF, containing 50 mmol LiBr, as eluent at a flow rate of 1 mL/min. Linear poly(methyl methacrylate) and polystyrene standards (PMMA from $M_p=440-1~650~000~g/mol$; PS from $M_p=666-2~300~000~g/mol$) were used.

2.3.3. Dynamic light scattering characterization (DLS)

DLS was used to determine the average hydrodynamic diameters of the obtained Ag nanoparticles. Measurements were performed on Zetasizer Nano ZS90 analyzer using Malvern Zetasizer Software 7.11. Measurements were done in DMSO at 20 $^{\circ}\text{C}$ using quartz glass cuvettes with 10 mm path length.

2.3.4. UV-Vis characterization

To study optical properties of obtained hybrid silver nanoparticles

the UV–Vis analysis was performed at room temperature using a Thermo Scientific Evolution 220 UV–Vis spectrophotometer with 1 nm resolution. The standard quartz cuvettes with the 10 mm of optical pathway were used and spectra were collected relative to the pure solvent as reference.

2.3.5. SERS performance

Raman spectra with the spectral resolution of c.a. $0.5~cm^{-1}$ were acquired with a dispersive Raman spectrometer T64000 (Jobin Yvon) equipped with Olympus B-40 microscope. The long working distance objective (x50, NA = 0.5) was used. An argon laser line 514.5 nm was applied for sample excitation. Laser power of 0.6 mW was measured on the sample surface. Acquisition time was 2 x 15 s. The SERS samples were prepared by the drop-casting of Ag@template nanoobjects mixed with crystal violet solutions in DMSO (used concentrations of CV: 10 mM, 0.1 mM, 0.01 mM) to obtain final concentrations of CV for each sample: 200 μ M, 2 μ M and 200 nM. Immediately after mixing, the solutions were deposited onto chromed copper plates through the dropcasting method and covered to protect the solvent against rapid evaporation. The droplets were left for complete solvent evaporation. The dry layers were examined by Raman spectroscopy. The results presented for each sample were obtained for at least three independent measurements.

2.3.6. High-resolution transmission electron microscopy characterization (HR-TEM)

JEOL ARM 200F was used to investigate the morphology of hybrid silver nanoparticles via HR-TEM. Before HR-TEM measurements, approximately 40 μL of the nanoparticles' dispersions were dropped on the carbon-coated copper grids that were covered with an ultrathin carbon layer from Ted Pella. The samples were allowed to dry under ambient conditions for a minimum of 12 h and then observed using a JEOL ARM 200F microscope operating at 200 kV. Concentration of the nanoparticles' dispersions was around 0.33 mg/mL.

3. Results and discussion

3.1. Characterization of polymer templates

Molecular templates with varied topology, meaning different numbers and degree of polymerization of arms were prepared using atom transfer radical polymerization (ATRP). First, 1,1,1-tris(4-hydroxyphenyl) ethane (THPE) and poly (2-(trimethylsilyloxy)ethyl methacrylate) P(HEMA-TMS) were modified using α-bromoisobutyryl bromide (BIBB), obtaining 1,1,1-tris(4-2-bromoisobutyryloxy)phenyl)ethane (TBPE) and poly(2-bromoisobutyryloxyethyl methacrylate) (PBiBEM) initiators, respectively (Fig. 1A). Then, block copolymer arms, poly(tertbutyl acrylate)-block-polystyrene (PtBA-b-PS) were synthesized using "grafting from" approach, followed by the hydrolysis of tBA units to obtain copolymers containing acrylic acid (AA) (PAA-b-PS) (Fig. 1B). To generate silver nanoparticles in the last step, silver nitrate was used as silver precursor. It was incorporated within the star-like templates due to the interactions between carboxylate ions of PAA units and silver ions. Then, silver ions were reduced using sodium borohydride, leading to silver nanoparticle formation (Fig. 1C). Polystyrene that was used as an outer block of the arms provided stability to the templates loaded with nanoparticles.

Synthesized polymers were characterized using gel permeation chromatography and proton nuclear magnetic resonance. The evolution of molecular weight after each step of the template synthesis was presented for PBiBEM $_{17}$ -g-(PtBA $_{46}$ -b-PS $_{19}$), as an example (Fig. S1). The shift of the GPC curves after each step of star-like polymer synthesis as well as their symmetrical shape indicated the controlled character of the polymerizations. The chemical structure of the obtained PBiBEM $_{17}$ -g-(PAA $_{46}$ -b-PS $_{19}$) star-like polymer was confirmed based on 1 H NMR spectrum (Fig. S2). Signals of PBiBEM protons are invisible as the molar

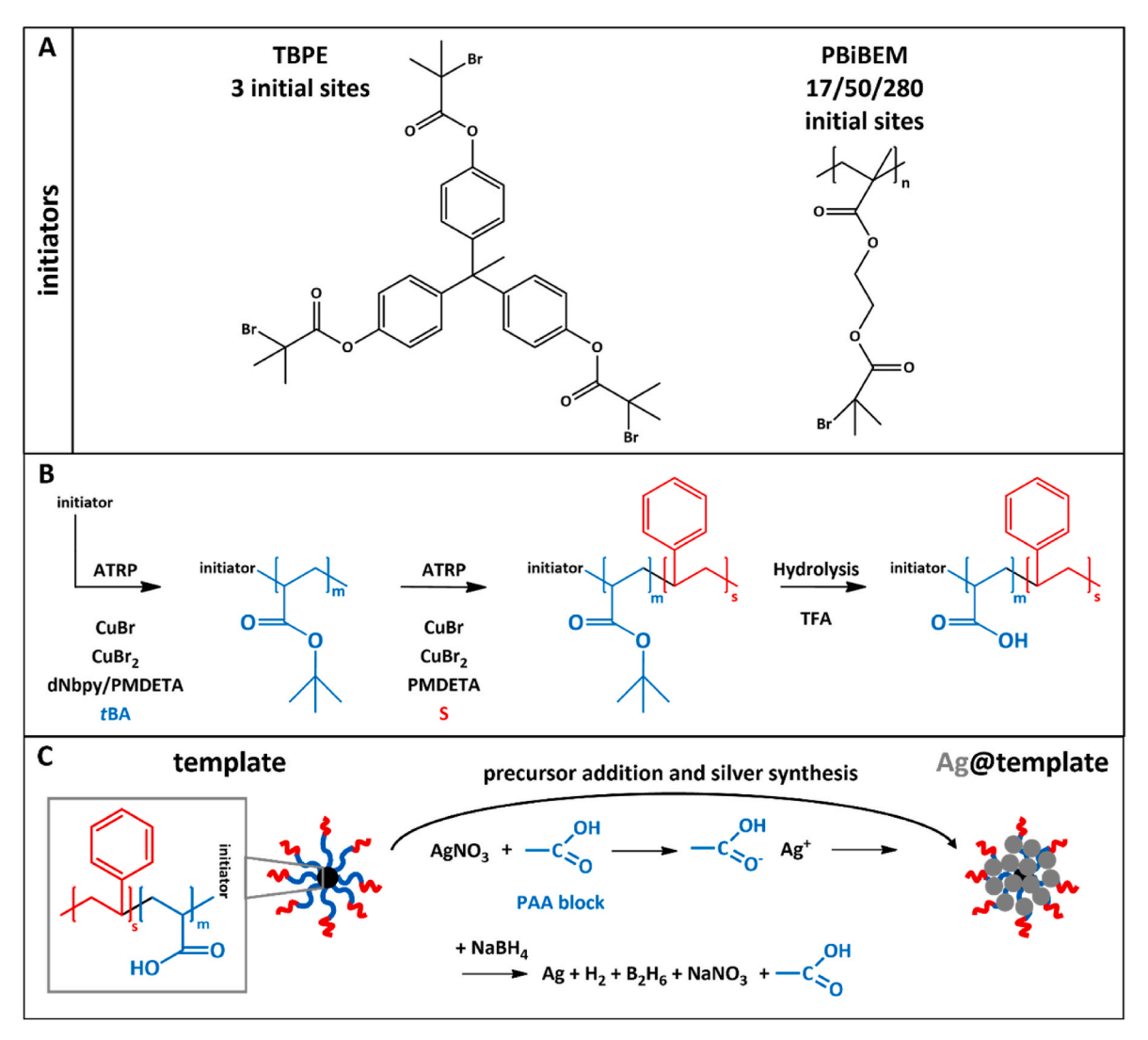


Fig. 1. (A) Initiators used for the preparation of (B) diblock copolymer containing templates and (C) synthesis of silver nanoparticles within the templates (Ag@template).

fraction of the arms is much higher than the core (they should appear at $\delta=0.70$ –2.35 ppm (a, b, e) and at $\delta=4.00$ –4.50 (c, d)). Methylene groups from the main PAA chain (f, g) and the main PS chain (i, j) overlapped each other in the range $\delta=0.70$ –2.35 ppm, while phenyl group from PS (k) appeared at $\delta=6.30$ –7.30 ppm. Successful hydrolysis of PtBA units was proved by the appearance of a new signal of proton of hydroxyl group in PAA structure (h) at $\delta=12.20$ ppm.

Four varied macroinitiators with 3, 17, 50, and 280 initiating sites were used for the preparation of a library of unimolecular templates. Synthesized PAA-b-PS arms had different lengths for each block, DP of PS block usually varied from 15 to 30. It was assumed that longer outer blocks could screen silver particles obtained in the core of the template, resulting in the limitation of the performance of these materials in SERS spectroscopy. The ratio of degree of polymerization of PAA and degree of polymerization of PS was usually around 2.4 and 3.6. Additionally, there were also prepared samples without PS protective block and with reversed order of the blocks (PS-b-PAA). Chemical composition, molecular weight, and dispersity for all prepared templates are presented in Table 1.

3.2. Characterization of hybrid nanoparticles

Nanoparticles were synthesized according to the general procedure, regardless of the template type (Fig. 1C) [14,15]. During the synthesis,

Table 1Molecular parameters of the synthesized molecular templates.

chemical composition ^a	$M_{ m n~NMR}^{ m a}$	$M_{\rm n}^{\rm b}$	$\boldsymbol{\mathit{D}}^{\mathrm{b}}$
TBPE-(PAA ₂₉ -b-PS ₆₆) ₃	27 650	41 700	1.24
TBPE-(PAA ₅₄ -b-PS ₂₃) ₃	28 700	36 300	1.22
TBPE- $(PAA_{80}-b-PS_{23})_3$	38 700	46 800	1.28
TBPE-(PAA ₈₇ -b-PS ₉) ₃	22 380	34 800	1.12
TBPE- $(PAA_{110})_3$	24 530	33 900	1.14
TBPE- $(PAA_{136}-b-PS_{29})_3$	62 100	56 800	1.06
$PBiBEM_{17}$ - g - $(PAA_{46}$ - b - $PS_{19})$	128 600	94 300	1.11
$PBiBEM_{17}$ - g - $(PAA_{80}$ - b - $PS_{21})$	216 200	188 000	1.09
PBiBEM ₁₇ -g-(PS ₂₂ -b-PAA ₈₆)	231 100	158 900	1.07
PBiBEM ₁₇ -g-PAA ₄₆	105 000	43 300	1.12
$PBiBEM_{50}$ - g - $(PAA_{47}$ - b - $PS_{20})$	419 300	207 800	1.46
PBiBEM ₂₈₀ -g-(PAA ₅₅ -b-PS ₃₉)	3 189 300	545 700	1.52

^a Degree of polymerization (DP) and theoretical molecular weight ($M_{n\ NMR}$) were calculated based on 1H NMR results.

the color of the reaction mixture changed from transparent to brown due to the reduction of silver ions to metallic silver. The successful synthesis of silver hybrid nanoparticles was also confirmed using the UV–Vis

^b Number average molecular weight (M_n) and dispersity (\mathcal{D}) were determined by GPC based on RI detector and PS standards for samples before PtBA hydrolysis.

spectroscopy. It was found, that both the position of the maximum and shape of the absorption peak strongly depend on the size of the nanoparticles (a broad peak suggests the presence of more than one nanoparticle fraction) [33]. Nanoparticles were also characterized by the DLS to determine their hydrodynamic diameters. Peak maxima from UV–Vis and diameters from DLS registered for all investigated systems are summarized in Table 2. Graphical data for hybrid nanoparticles obtained from all templates are presented in Supporting Information (Figs. S3–S14).

Based on the UV–Vis spectroscopy and DLS results it was found that three-arm star polymers enabled the synthesis of stable silver nanoparticles when the ratio of the template (-COO groups in PAA) to silver precursor (Ag⁺ from AgNO₃) was 2:1 and 1:1. For all hybrid nanoparticles size varied from 15 to 25 nm (Figs. S3–S8, Fig. 2A) and no dependence between diameter and arm length was observed. This suggests the partial aggregation of hybrid nanoparticles as a result of strong interactions between them. Nevertheless, most of the samples were stable after the synthesis for more than one year. On the contrary, the formation of the aggregates and precipitation of silver during the syntheses was observed when -COO:Ag⁺ ratio was 1:2. When DP_{PS} was increased, while DP_{PAA} was decreased in the TBPE-(PAA₂₉-b-PS₆₆)₃ template, samples stability decreased, and aggregation was observed (Fig. S3). Probably PS blocks formed a layer that limited the

 Table 2

 Characterization of hybrid silver particles (Ag@template).

template composition	-COO ⁻ : Ag ⁺	absorption peak maximum (nm) ^a	hydrodynamic diameter (nm) ^b
		, ,	` ´
TBPE-(PAA ₂₉ -b-	2:1	415	$10 \pm 3; 52 \pm 23$
PS ₆₆) ₃	1:1	420	156 ± 66
	1:2 ^d	N/A	N/A
TBPE-(PAA ₅₄ -b-	2:1	413	22 ± 5
PS ₂₃) ₃	1:1	413	20 ± 5
	1:2	418	24 ± 5
TBPE-(PAA ₈₀ -b-	2:1	426	21 ± 10
$PS_{23})_3$	1:1	421	20 ± 9
	1:2 ^d	N/A	N/A
TBPE-(PAA ₈₇ -b-	2:1	411	17 ± 5
$PS_9)_3$	1:1	411	21 ± 8
	1:2	412	$10\pm3;58\pm32$
TBPE- $(PAA_{110})_3$	4:1	416	4 ± 1
	2:1 ^e	422 ^c	171 ± 53
	1:1 ^e	445 ^c	$98 \pm 25;730 \pm 252$
	1:2 ^d	N/A	N/A
TBPE-(PAA ₁₃₆ -b-	2:1	413	19 ± 6
$PS_{29})_3$	1:1	414	18 ± 11
	1:2 ^d	N/A	N/A
PBiBEM ₁₇ -g-	2:1	421	6 ± 1
$(PAA_{46}-b-PS_{19})$	1:1	423	5 ± 1
	1:2	420	4 ± 1
PBiBEM ₁₇ -g-	2:1	406	4 ± 1
(PAA ₈₀ -b-PS ₂₁)	1:1	408	2 ± 1
	1:2 ^d	N/A	N/A
PBiBEM ₁₇ -g-(PS ₂₂ -	2:1	417	41 ± 10
b-PAA ₈₆)	1:1	417	48 ± 10
	1:2	417	40 ± 8
PBiBEM _{1.7} -g-PAA ₄₆	2:1 ^e	412 ^c	72 ± 25
-, 0	1:1 ^e	413 ^c	166 ± 54
	1:2 ^d	N/A	N/A
PBiBEM50-g-	2:1 ^d	N/A	N/A
(PAA ₄₇ -b-PS ₂₀)	1:1	422	40 ± 19
, 207	1:2	411	34 ± 8
PBiBEM ₂₈₀ -g-	2:1	418	$15 \pm 4; 119 \pm 63$
(PAA ₅₅ -b-PS ₃₉)	1:1	422	$26 \pm 8; 164 \pm 95$
. 55 53	1:2 ^d	N/A	N/A

 $^{^{\}rm a}$ Determined by UV–Vis in DMSO at 25 $^{\circ}\text{C}.$

incorporation of the precursor into PAA units, so silver nanocrystals were formed mostly outside of the template and aggregated.

Star-like polymers with 17 arms, PBiBEM $_{17}$ -g-(PAA $_{46}$ -b-PS $_{19}$) and PBiBEM $_{17}$ -g-(PAA $_{80}$ -b-PS $_{21}$), provided the best stability of hybrid nanoparticles. The hydrodynamic diameter of the obtained hybrid silver nanoparticles was a few nanometers (Figs. S9–S10), which was smaller than expected, however, some aggregates with a diameter of around 50 nm were also observed (Fig. 2B). Introducing PS as an inner block in the arm, PBiBEM $_{17}$ -g-(PS $_{22}$ -b-PAA $_{86}$), also resulted in the formation of well-defined stable nanoparticles but their hydrodynamic diameters were in the range of 40–50 nm due to the strong interactions between outer PAA blocks leading to aggregation (Fig. S11). Noteworthy is the fact that nanoparticles were stable for almost two years after the synthesis.

The necessity to use a PS block was confirmed by preparing silver nanoparticles using templates including only PAA block, TBPE-(PAA $_{110}$)₃ and PBiBEM $_{17}$ -g-PAA $_{46}$, respectively. Formed particles aggregated and precipitated during the synthesis that was monitored by DLS (Figs. S7 and S12). Stable nanoparticles were synthesized using TBPE-(PAA $_{110}$)₃ only when a low amount of the precursor was used, -COO*:Ag* = 4:1, however, no SERS was observed for this nanomaterial in further measurements.

Silver hybrid nanoparticles synthesized within the template containing a higher number of arms than 17, PBiBEM $_{50}$ -g-(PAA $_{47}$ -b-PS $_{20}$), were stable when ratio -COO':Ag $^+$ was 1:1 and 1:2. Nanoparticles had diameters in the range of 30–40 nm (Fig. S13), while on HR-TEM images, NPs' size was slightly lower (Fig. 2C). Furthermore, if AgNPs was synthesized using PBiBEM $_{280}$ -g-(PAA $_{55}$ -b-PS $_{39}$) templates, a bimodal distribution of nanoparticle sizes was obtained. The fraction with a hydrodynamic diameter of 15–25 nm was formed outside of the template, while the main fraction had an average diameter of around 175 nm (Fig. S14, Fig. 2D). These results are in agreement with data reported for the synthesis of TiO $_2$ within molecular brush templates [24].

3.3. Hybrid silver nanoparticles as SERS substrates

Synthesized hybrid nanoparticles Ag@template were investigated as potential SERS substrates using crystal violet (CV) as an analyte. This substance is a widely used organic dye, not only in the textile industry but also in medicine due to its fungicidal and bactericidal properties [34–36]. For the sake of widespread use, it is now one of the common water pollutants exhibiting toxic, genotoxic, and carcinogenic behaviors [37–40]. Therefore, new analytical methods capable of detecting substances with concentrations in the nanomolar range are currently being searched for. The SERS technique seems to be appropriate in this field because of the low detection limit. Moreover, the CV is often used as a model target molecule in the investigation of the SERS effect [41,42] and has a high affinity to silver nanoparticles.

The characteristic peaks for crystal violet appearing in the regions: 935 cm⁻¹ ring skeletal vibrations, 1175 cm⁻¹ C–H in-plane bending vibrations, 1390 cm⁻¹ N-phenyl stretching vibrations, 1549, 1591 and 1622 cm⁻¹ C–C stretching vibrations [43,44]. The peak at 1622 cm⁻¹ was selected for Enhancement Factor (EF) calculations as the most intense one. EF was calculated according to the equation [45]:

$$EF = (I_{SERS} \cdot C_{Raman})/(I_{Raman} \cdot C_{SERS})$$
(1)

where: I_{SERS} and I_{Raman} are intensities of the CV peak on spectrum recorded in the presence of silver hybrid nanoparticles (SERS conditions), and in the layer drop-casted from the DMSO solution (standard Raman experiment), while C_{SERS} and C_{Raman} are CV concentrations in the sample with silver hybrid nanoparticles and in DMSO solution, respectively. All EF results are summarized in Table S2.

3.3.1. Effect of silver amount

An influence of silver content within hybrid nanoparticles on SERS effect is presented in Fig. 3 using Ag@PBiBEM₁₇-g-(PAA₄₆-b-PS₁₉) as an

 $^{^{\}rm b}$ Hydrodynamic diameters (volume distribution) were determined by DLS in DMSO at 20 $^{\circ}\text{C}.$

^c Broad peak on UV–Vis spectrum suggesting nanoparticles' aggregation and/or agglomeration.

^d Sample precipitated during or shortly after the synthesis.

^e Sample was stable for 48 h and later it precipitated.

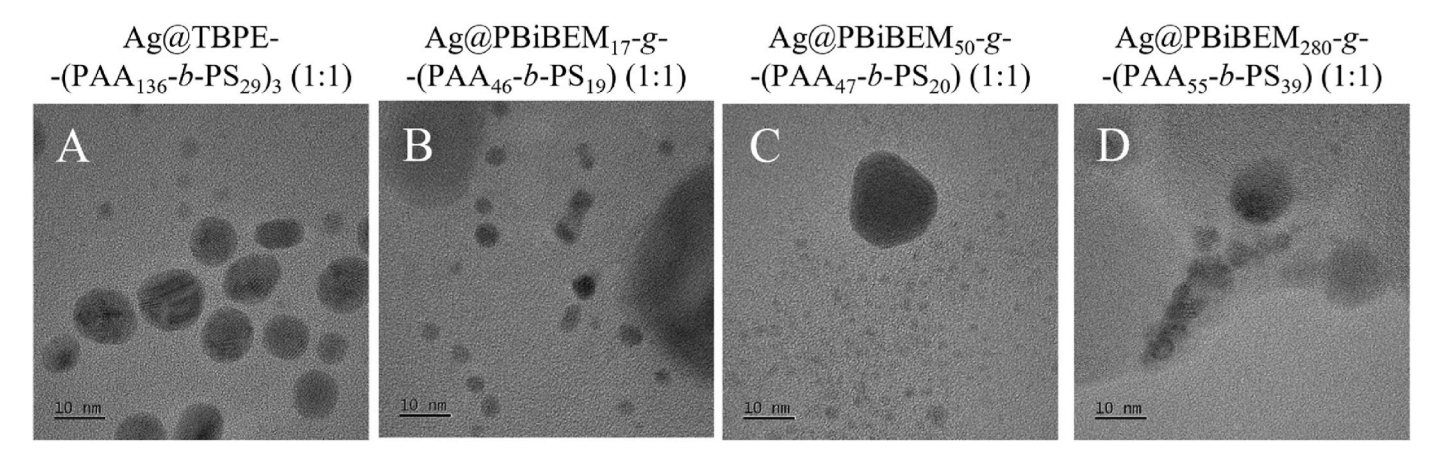


Fig. 2. HR-TEM images of nanoparticles obtained using different molecular templates: (A) TBPE-(PAA₁₃₆-b-PS₂₉)₃, (B) PBiBEM₁₇-g-(PAA₄₆-b-PS₁₉), (C) PBiBEM₅₀-g-(PAA₄₇-b-PS₂₀), (D) PBiBEM₂₈₀-g-(PAA₅₅-b-PS₃₉). The scale bar is 10 nm.

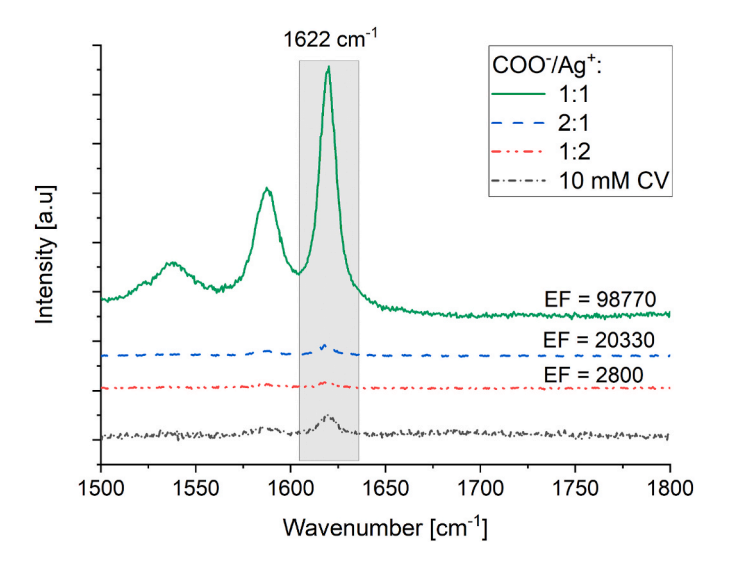


Fig. 3. SERS spectra of CV deposited onto $Ag@PBiBEM_{17}$ -g-(PAA_{46} -b- PS_{19}) hybrid nanoparticles with different molar ratios of -COO: Ag^+ . The CV concentration was 2 μ M. CV spectrum was added as a reference.

arbitrarily chosen example. The best results (the highest EF) were obtained for the samples with a -COO to Ag+ ratio of 1:1. This trend was observed for other tested systems and also in our previous works where the polymer templates for the synthesis of Ag nanoparticles were created by PISA [14,15]. Despite the various size of the templates (a dozen nanometers in the case of star-like polymer discussed within this work vs. tens of nanometers for PISA systems) the optimal Ag⁺ content for the preparation of the most effective SERS supports is equimolar with carboxyl groups. It means that the -COO to Ag+ ratio is the crucial parameter determining the SERS effectiveness of investigated materials independently of the polymer template shape and size. The observed effect can be explained considering that for the higher silver concentration, aggregates of silver nanoparticles were created resulting in the reduction of silver surface accessible for CV molecules and a reduction of the number of hot spots in the system. Thus, the SERS signals for systems with a -COO to Ag+ ratio of 1:2 are usually weaker in comparison to systems with a -COO to Ag+ ratio of 1:1. If the -COO to Ag+ ratio is 2:1, the amount of silver is insufficient to create many NPs in close proximity (the distances between silver nanoparticles inside the polymer template are too high to create numerous hot spots), and SERS signal is low.

3.3.2. Effect of the number of arms

TBPE-(PAA₅₄-b-PS₂₀)₃, PBiBEM₁₇-g-(PAA₄₆-b-PS₁₉), and PBiBEM₅₀-

g-(PAA₄₇-b-PS₂₀) systems can be used to discuss the impact of a number of arms in polymer template on the SERS effectiveness of final hybrid nanoparticles. These templates have similar DP_{PAA}:DP_{PS} ratio equals 2.4 so the main difference between them is the number of arms in each system. For comparison the systems with -COO:Ag $^+$ ratio 1:1 were used. Representative SERS spectra are presented in Fig. 4. For the stars with 3 arms the SERS effect is much weaker compared to the others. It is due to the fact, that they act the same as linear polymers so there is no possibility to create hot spots – AgNPs are too far away from each other.

Not only too little number of arms in a polymer star-like template but also too many seem to be inappropriate for effective SERS support, because hybrid nanoparticles prepared based on a 50-arm-star gave smaller enhancement than the hybrid nanoparticles containing a 17-arm-star template. This behavior can be interpreted as a result of the limited penetrability of so dense polymer system by analyte molecules.

3.3.3. Block order effect

Systems with the same number and length of arms but a different order of PAA and PS blocks were also analyzed (Fig. 5). The star-like polymer templates containing 17 arms were selected to create final hybrid nanoparticles and the average total arm length was close to 100. For comparison, the systems with a -COO⁻:Ag⁺ ratio of 1:1 were used.

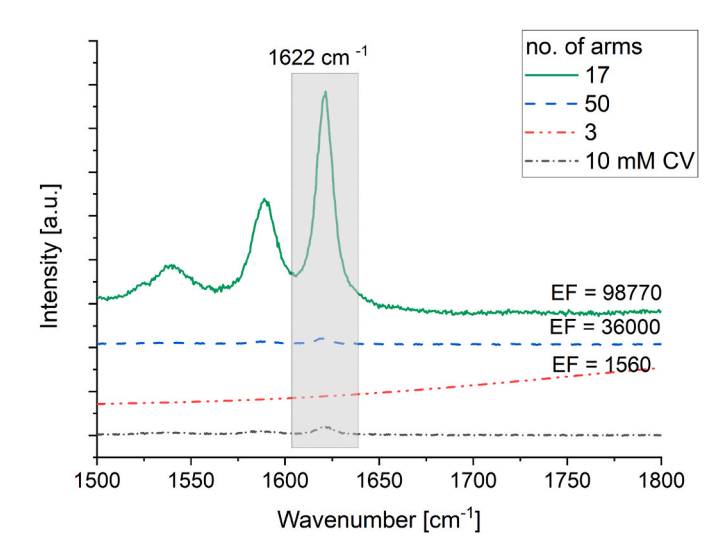


Fig. 4. SERS spectra of CV deposited onto Ag@TBPE-(PAA $_{54}$ -b-PS $_{20}$) $_3$, Ag@P-BiBEM $_{17}$ -g-(PAA $_{46}$ -b-PS $_{19}$) and Ag@PBiBEM $_{50}$ -g-(PAA $_{47}$ -b-PS $_{20}$) hybrid nanoparticles with -COO':Ag $^+$ = 1:1 ratio. The spectrum of CV measured under standard (non-SERS) conditions was added for comparison. The CV concentration was 2 μ M.

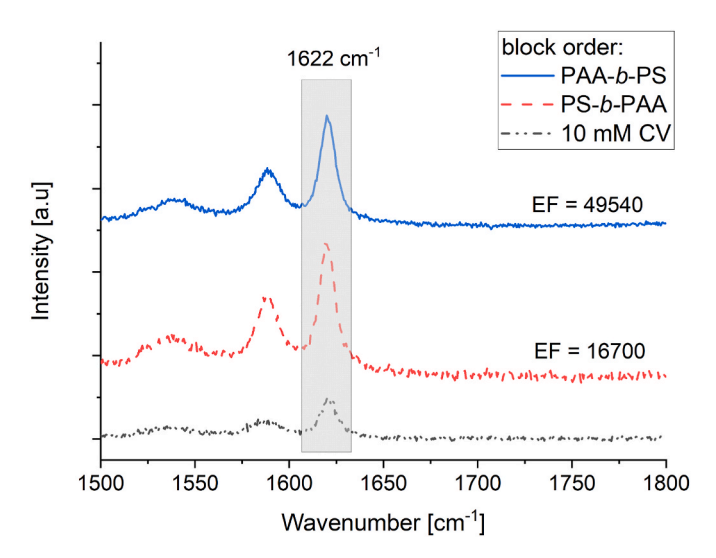


Fig. 5. SERS spectra of CV deposited onto $Ag@PBiBEM_{17}$ -g- $(PS_{22}$ -b- $PAA_{86})$ and $Ag@PBiBEM_{17}$ -g- $(PA_{80}$ -b- $PS_{21})$ hybrid nanoparticles with -COŌ: $Ag^+=1:1$ ratio. The spectrum of CV measured under standard (non-SERS) conditions was added for comparison. The CV concentration was 2 μ M.

Surprisingly, it was found that the order of the PAA and PS blocks is not a crucial parameter determining the SERS effect, as for both tested systems the enhancement was relatively high. The EF was higher if polystyrene was placed in the exterior part of the hybrid nanoparticle (Ag@PBiBEM₁₇-g-(PAA₈₀-b-PS₂₁) system) although it was expected that the silver nanoparticles could be less accessible for CV molecules if they are in the inner layer of polymer template. These results show the significant role of stabilizing hydrophobic (polystyrene) blocks in polymer templates that are required to protect the final nanoparticles against agglomeration. For a system with PAA outer blocks (Ag@PBiBEM17-g-(PS₂₂-b-PAA₈₆)), strong interactions between nanoparticles were expected resulting in potential agglomeration and reduction of silver surface accessibility for analyte molecules. Overall, it means that the design of effective SERS supports based on star-like polymer templates requires consideration of both indeed contradictory structural effects: silver surface accessibility - higher if the PAA forms the outer layer, and hybrid nanoparticle stability - higher if the PS forms the outer layer.

3.3.4. Effect of PAA and PS blocks length ratio

One of the crucial parameters determining the amount of silver possible to be loaded into a star-like polymer template is the relative length of both blocks: with high affinity to silver ions (PAA in case of systems tested herein) and with low affinity to Ag $^+$ ions (PS block). Thus, the ratio of $\mathrm{DP}_{\mathrm{PAA}}.\mathrm{DP}_{\mathrm{PS}}$ should strongly affect the Enhancement Factor. Fig. 6 shows SERS spectra of CV deposited onto the hybrid nanoparticles prepared based on star-like polymer templates with $\mathrm{DP}_{\mathrm{PAA}}.\mathrm{DP}_{\mathrm{PS}} = 2.4$ or 3.8. It was observed that the SERS effect decreased with the increase of the $\mathrm{DP}_{\mathrm{PAA}}.\mathrm{DP}_{\mathrm{PS}}$ ratio.

3.3.5. Effect of the analyte concentration (detection limit)

The detection limit (the lowest concentration of the analyte that can be detected) is a fundamental point determining the applicability of the given analytical method. For some SERS systems, the detection limit was found even at the picomolar level [46], but most works report that the useful systems work on the nanomolar level [33,47]. Thus, the system that exhibited the highest EF, namely Ag@PBiBEM17-g-(PAA46-b-PS19) with -COO:Ag^+ = 1:1, was investigated for the detection limit (Fig. 7). Measurements conditions were changed to obtain a better quality of results (laser power 0.1 mW, acquisition time 1 \times 180 s). SERS measurements showed high sensitivity of the polymer hybrids as a substrate for CV analysis, which allowed the detection of CV in solutions of concentration as low as 2 nM. This value is very similar to the values

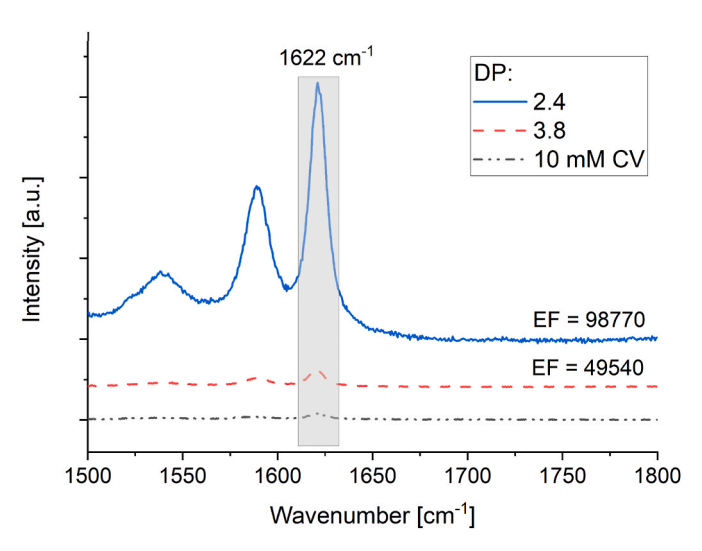


Fig. 6. SERS spectra of $Ag@PBiBEM_{17}$ -g-(PAA_{46} -b- PS_{46}), $Ag@PBiBEM_{17}$ -g-(PAA_{80} -b- PS_{21}), with -COO: $Ag^+=1:1$ ratio. The spectrum of CV measured under standard (non-SERS) conditions was added for comparison.

reported for other systems [42,48].

3.3.6. Aging effect

It is commonly known that nanoparticles have high surface energy and due to that their stability is usually limited. In dispersion, they tend to agglomerate and/or aggregate which may negatively impact their properties, including SERS effectiveness [49,50]. In the systems discussed herein, the silver nanocrystals are introduced and chemically attached to the polymer template that stabilizes them. Nevertheless, agglomeration may occur at the level of whole hybrid nanoparticles reducing the silver surface accessibility and SERS strength. Thus, the influence of aging was also investigated. Even after 5 months of storage of the dispersion of hybrids particles under room temperature and in darkness, the sample $Ag@PBiBEM_{17}$ -g- $(PS_{22}$ -b- $PAA_{86})$ was still able to serve as an effective SERS substrate (Fig. 8). Comparison of SERS spectra recorded for the "fresh" hybrid nanoparticles and 5-months aged ones shows that the intensity of the CV band at 1622 cm⁻¹ was only slightly lower in the aged system, within experimental error. These results prove the effectiveness and very high stability of the synthesized hybrid nanoparticles as SERS substrates.

4. Conclusions

New, stable, hybrid polymer star-like/silver nanoparticles were proposed as effective SERS supports. The core-first strategy was used to synthesize well-defined star-like copolymers by ATRP. Synthesized macromolecules varied on the number of arms, order of blocks of high (PAA) and low (PS) affinity to silver ions, as well as the ratio between the degree of polymerization of PAA and PS blocks.

It was shown that the number of arms in a polymer template was a crucial parameter determining the SERS effectiveness of hybrid nanoparticles. If the number of arms was too low the hot spots formation between silver particles was very limited leading to a low SERS effect. On the contrary, the too-high number of arms of the templates resulted in high polymer density within single hybrid particles, which limited the penetrability of hybrid nanoparticles by analyte molecules. The optimal density of arms should allow penetration of analyte inside the hybrid particles and simultaneously give a possibility to form hot spots by silver nanocrystals.

Contrarily to the number of arms, the order of blocks within a single arm played a secondary role in SERS. It is probably because of two negative effects, which impacted the silver surface accessibility: agglomeration of hybrid nanoparticles that was promoted if the PAA

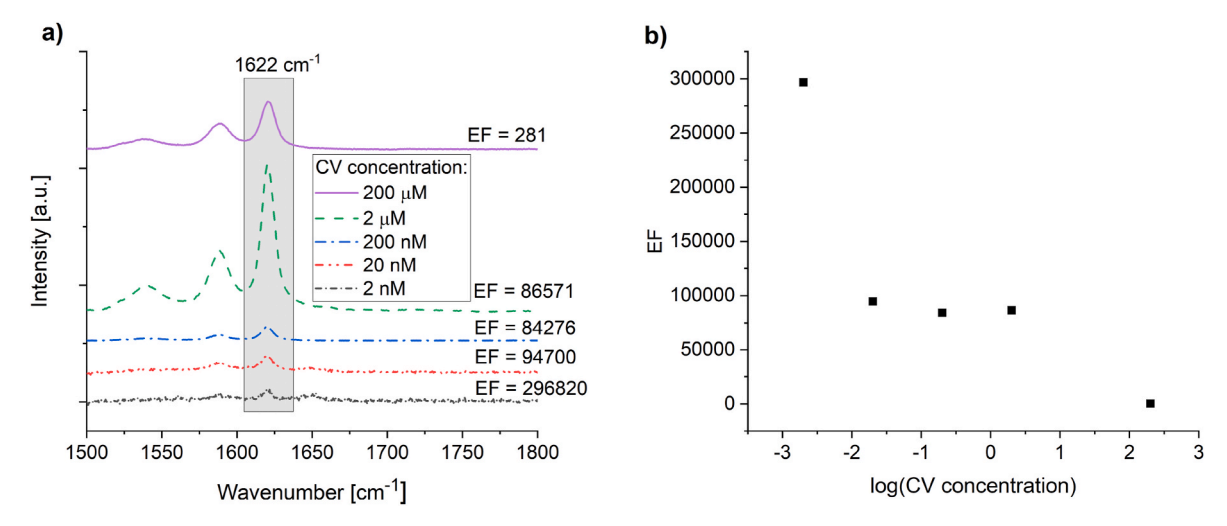


Fig. 7. A) SERS spectra of CV deposited onto Ag@PBiBEM $_{17}$ -g-(PAA $_{46}$ -b-PS $_{19}$) with -COO $^{\cdot}$ Ag $^{+}=1:1$. Spectra for 2 nM and 20 nM were multiplied by 20 and 10, respectively. b) Calculated enhancement factor as a function of CV concentration.

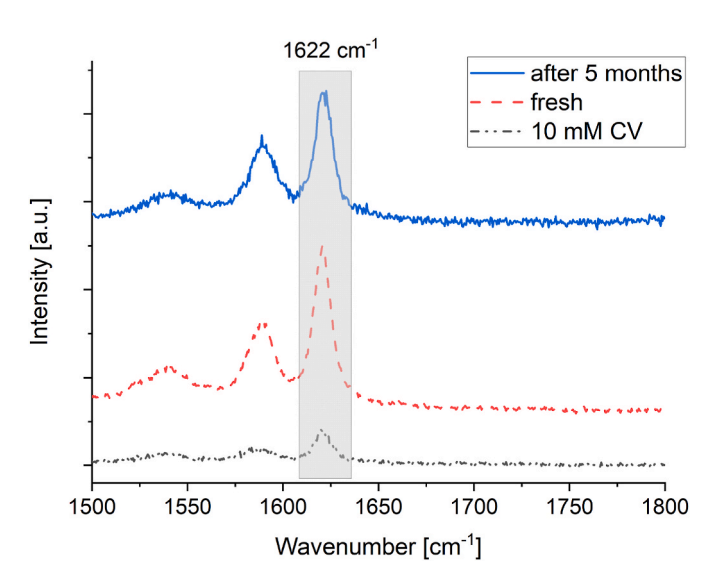


Fig. 8. SERS spectra of CV deposited onto Ag@PBiBEM $_{17}$ -g-(PS $_{22}$ -b-PAA $_{86}$) hybrid nanoparticles with -COO:Ag $^+$ = 1:2, before and after five months of storage. The CV concentration was 2 μ M.

block was the exterior of the template and diffusion pathway of analyte molecule inside the hybrid nanocomposite that could be limited if PS was an outer layer and its degree of polymerization was too high.

It was also observed that the SERS effect decreased with the increase of the $\mathrm{DP}_{\mathrm{PAA}}$: $\mathrm{DP}_{\mathrm{PS}}$ ratio. The optimal content of the silver nanoparticles, that were generated within the template, was obtained if the molar ratio between the carboxylic group of polymer templates and silver particles precursor was 1:1. This ratio seems to be universal for PS-PAA templates independent of their size and morphology, as the identical value was previously found for PS-PAA templates obtained by PISA [14,15].

It is important to highlight, that $Ag@PBiBEM_{17}\text{-}g\text{-}(PAA_{46}\text{-}b\text{-}PS_{19})$ hybrid particles, which were the most efficient system for SERS, allowed the detection of the analytes on the nanomolar level. It provides new perspectives for the applications of similar materials in analytical practice.

Finally, the high stability of tested systems was shown, as the EF measured for fresh and aged five months samples was the same.

CRediT authorship contribution statement

Krzysztof Jerczynski: Investigation, Methodology, Formal analysis, Writing – original draft. Julita Muszynska: Investigation, Methodology, Formal analysis, Writing – original draft. Gokhan Demirci: Investigation. Onur Cetinkaya: Investigation. Paulina Filipczak: Investigation, Formal analysis, Writing – original draft. Grzegorz Nowaczyk: Investigation. Jaroslaw Grobelny: Methodology. Krzysztof Matyjaszewski: Conceptualization, Writing – review & editing. Marcin Kozanecki: Conceptualization, Methodology, Writing – review & editing, Supervision. Joanna Pietrasik: Conceptualization, Methodology, Writing – review & editing, Supervision.

Declaration of competing interest

The authors declare that they have no known competing financial interests or personal relationships that could have appeared to influence the work reported in this paper.

Data availability

Data will be made available on request.

Acknowledgment

K.J., J.M., G.D., O.C., P.F., M.K., K.M. and J.P. acknowledge the financial support from National Science Center, Poland (via Grant UMO-2014/14/A/ST5/00204). K.M. acknowledges support from NSF (CHE 2108901).

Appendix A. Supplementary data

Supplementary data to this article can be found online at https://doi.org/10.1016/j.polymer.2023.126363.

References

- Y.L. Wang, J. Irudayaraj, Surface-enhanced Raman spectroscopy at single-molecule scale and its implications in biology, Phil, Trans. Biol. Sci. 368 (1611) (2013).
- scale and its implications in biology, Phil. Trans. Biol. Sci. 368 (1611) (2013).
 [2] L.L. Yang, Y. Yang, Y.F. Ma, S. Li, Y.Q. Wei, Z.R. Huang, N.V. Long, Fabrication of semiconductor ZnO nanostructures for versatile SERS application, Nanomaterials 7 (11) (2017)
- [3] P.G. Etchegoin, E.C. Le Ru, A perspective on single molecule SERS: current status and future challenges, Phys. Chem. Chem. Phys. 10 (40) (2008) 6079–6089.
- [4] E.C. Le Ru, P.G. Etchegoin, Single-molecule surface-enhanced Raman spectroscopy, Annu. Rev. Phys. Chem. 63 63 (2012) 65–87.

- [5] R.C. Maher, C.M. Galloway, E.C. Le Ru, L.F. Cohena, P.G. Etchegoin, Vibrational pumping in surface enhanced Raman scattering (SERS), Chem. Soc. Rev. 37 (5) (2008) 965–979.
- [6] Y. Yu, T.H. Xiao, Y.Z. Wu, W.J. Li, Q.G. Zeng, L. Long, Z.Y. Li, Roadmap for single-molecule surface-enhanced Raman spectroscopy, Adv. Photonics 2 (1) (2020).
- [7] R.C. Maher, Raman Spectroscopy for Nanomaterials Characterization SERS Hot Spots, Springer-Verlag Berlin Heidelberg, 2012.
- [8] J.L. Yang, H.J. Wang, H. Zhang, Z.Q. Tian, J.F. Li, Probing hot electron behaviors by surface-enhanced Raman spectroscopy, Cell Rep. Phys. Sci. 1 (9) (2020).
- [9] X. Pang, L. Zhao, W. Han, X. Xin, Z. Lin, A general and robust strategy for the synthesis of nearly monodisperse colloidal nanocrystals, Nat. Nanotechnol. 8 (2013) 426
- [10] H.D. Koh, N.G. Kang, J.S. Lee, Location control of Au/CdS nanoparticles in block copolymer micelles, Langmuir 23 (23) (2007) 11425–11429.
- [11] J.M. Hu, Y.F. Qian, X.F. Wang, T. Liu, S.Y. Liu, Drug-loaded and superparamagnetic iron oxide nanoparticle surface-embedded amphiphilic block copolymer micelles for integrated chemotherapeutic drug delivery and MR imaging, Langmuir 28 (4) (2012) 2073–2082.
- [12] N. Semagina, E. Joannet, S. Parra, E. Sulman, A. Renken, L. Kiwi-Minsker, Palladium nanoparticles stabilized in block-copolymer micelles for highly selective 2-butyne-1,4-diol partial hydrogenation, Appl. Catal. Gen. 280 (2) (2005) 141–147
- [13] X. Li, J. Iocozzia, Y.H. Chen, S.Q. Zhao, X. Cui, W. Wang, H.F. Yu, S.L. Lin, Z.Q. Lin, From precision synthesis of block copolymers to properties and applications of nanoparticles, Angew. Chem. Int. Ed. 57 (8) (2018) 2046–2070.
- [14] Y. Zhang, P. Filipczak, G. He, G. Nowaczyk, L. Witczak, W. Raj, M. Kozanecki, K. Matyjaszewski, J. Pietrasik, Synthesis and characterization of Ag NPs templated via polymerization induced self-assembly, Polymer 129 (2017) 144–150.
- [15] G. Demirci, J. Muszyńska, O. Cetinkaya, P. Filipczak, Y. Zhang, G. Nowaczyk, K. Halagan, J. Ulanski, K. Matyjaszewski, J. Pietrasik, M. Kozanecki, Effective SERS materials by loading Ag nanoparticles into poly(acrylic acid-stat-acrylamide)block-polystyrene nano-objects prepared by PISA, Polymer 224 (2021), 123747.
- [16] X.Y. Liu, C. Zhang, J.M. Yang, D.L. Lin, L. Zhang, X. Chen, L.S. Zha, Silver nanoparticles loading pH responsive hybrid microgels: pH tunable plasmonic coupling demonstrated by surface enhanced Raman scattering, RSC Adv. 3 (10) (2013) 3384–3390.
- [17] R.M. Jin, M.H. Yao, J. Yang, D.H. Zhao, Y.D. Zhao, B. Liu, One-step in situ synthesis of polypeptide-gold nanoparticles hybrid nanogels and their application in targeted photoacoustic imaging, ACS Sustain. Chem. Eng. 5 (11) (2017) 9841–9847.
- [18] Y.J. Liu, J.L. Wang, M.Y. Zhang, H.M. Li, Z.J. Lin, Polymer-ligated nanocrystals enabled by nonlinear block copolymer nanoreactors: synthesis, properties, and applications, ACS Nano 14 (10) (2020) 12491–12521.
- [19] Y. Chen, Y.J. Yoon, X. Pang, Y. He, J. Jung, C. Feng, G. Zhang, Z. Lin, Precisely size-tunable monodisperse hairy plasmonic nanoparticles via amphiphilic star-like block copolymers, Small 12 (48) (2016) 6714–6723.
- [20] X.C. Pang, Y.J. He, J.H. Jung, Z.Q. Lin, 1D nanocrystals with precisely controlled dimensions, compositions, and architectures, Science 353 (6305) (2016) 1268–1272
- [21] Y. Chen, D. Yang, Y.J. Yoon, X. Pang, Z. Wang, J. Jung, Y. He, Y.W. Harn, M. He, S. Zhang, G. Zhang, Z. Lin, Hairy uniform permanently ligated hollow nanoparticles with precise dimension control and tunable optical properties, J. Am. Chem. Soc. 139 (37) (2017) 12956–12967.
- [22] K. Budzalek, H. Ding, L. Janasz, A. Wypych-Puszkarz, O. Cetinkaya, J. Pietrasik, M. Kozanecki, J. Ulanski, K. Matyjaszewski, Star polymer–TiO2 nanohybrids to effectively modify the surface of PMMA dielectric layers for solution processable OFETs, J. Mater. Chem. C 9 (4) (2021) 1269–1278.
- [23] A. Łuczak, W. Waliszewski, K. Jerczyński, A. Wypych-Puszkarz, J. Rogowski, J. Pietrasik, M. Kozanecki, J. Ulański, K. Matyjaszewski, Continuity of thin layers of an organic semiconductor induced by the modification of the gate insulator, J. Mater. Chem. C 10 (41) (2022) 15541–15553.
- [24] K. Jerczynski, M. Lipinska, W. Raj, M. Šlouf, K. Halagan, M. Kozanecki, J. Grobelny, K. Matyjaszewski, J. Pietrasik, Effect of hybrid TiO2 nanoparticles with controlled morphology on rheological properties of poly(styrene-coacrylonitrile) nanocomposites, Mater. Today Chem. 26 (2022), 101189.
- [25] K. Matyjaszewski, N.V. Tsarevsky, Nanostructured functional materials prepared by atom transfer radical polymerization, Nat. Chem. 1 (4) (2009) 276–288.
- [26] K. Matyjaszewski, Advanced materials by atom transfer radical polymerization, Adv. Mater. 30 (23) (2018).
- [27] K. Matyjaszewski, N.V. Tsarevsky, Macromolecular engineering by atom transfer radical polymerization, J. Am. Chem. Soc. 136 (18) (2014) 6513–6533.

[28] K. Matyjaszewski, Atom transfer radical polymerization (ATRP): current status and future perspectives, Macromolecules 45 (10) (2012) 4015–4039.

- [29] K. Matyjaszewski, J.H. Xia, Atom transfer radical polymerization, Chem. Rev. 101 (9) (2001) 2921–2990.
- [30] K. Matyjaszewski, P.J. Miller, J. Pyun, G. Kickelbick, S. Diamanti, Synthesis and characterization of star polymers with varying arm number, length, and composition from organic and hybrid inorganic/organic multifunctional initiators, Macromolecules 32 (20) (1999) 6526–6535.
- [31] G. Xie, H. Ding, W.F.M. Daniel, Z. Wang, J. Pietrasik, S.S. Sheiko, K. Matyjaszewski, Preparation of titania nanoparticles with tunable anisotropy and branched structures from core–shell molecular bottlebrushes, Polymer 98 (2016) 481–486.
- [32] A. Nese, J. Mosnacek, A. Juhari, J.A. Yoon, K. Koynov, T. Kowalewski, K. Matyjaszewski, Synthesis, characterization, and properties of starlike poly(n-butyl acrylate)-b-poly(methyl methacrylate) block copolymers, Macromolecules 43 (3) (2010) 1227–1235.
- [33] J.M. Li, W.F. Ma, C.A. Wei, J. Guo, J. Hu, C.C. Wang, Poly(styrene-co-acrylic acid) core and silver nanoparticle/silica shell composite microspheres as high performance surface-enhanced Raman spectroscopy (SERS) substrate and molecular barcode label, J. Mater. Chem. 21 (16) (2011) 5992–5998.
- [34] A.M. Maley, J.L. Arbiser, Gentian Violet: a 19th century drug re-emerges in the 21st century, Exp. Dermatol. 22 (12) (2013) 775–780.
- [35] P. Bakker, H. Vandoorne, V. Gooskens, N.F. Wieringa, Activity of gentian-violet and brilliant green against some microorganisms associated with SKIN infections, Int. J. Dermatol. 31 (3) (1992) 210–213.
- [36] A. Talha Khalil, S. Hameed, S. Afridi, H.E.A. Mohamed, Z.K. Shinwari, Sageretia thea mediated biosynthesis of metal oxide nanoparticles for catalytic degradation of crystal violet dye, Mater. Today: Proc. 36 (2021) 397–400.
- [37] S. Mani, R.N. Bharagava, Exposure to crystal violet, its toxic, genotoxic and carcinogenic effects on environment and its degradation and detoxification for environmental safety, Rev. Environ. Contam. Toxicol. 237 237 (2016) 71–104.
- [38] M.R. Kulkarni, T. Revanth, A. Acharya, P. Bhat, Removal of Crystal Violet dye from aqueous solution using water hyacinth: equilibrium, kinetics and thermodynamics study, Res. Efficient Technol. 3 (1) (2017) 71–77.
- [39] F. Mashkoor, A. Nasar, Inamuddin, A.M. Asiri, Exploring the reusability of synthetically contaminated wastewater containing crystal violet dye using tectona grandis sawdust as a very low-cost adsorbent, Sci. Rep. 8 (2018).
- [40] A. Mittal, J. Mittal, A. Malviya, D. Kaur, V.K. Gupta, Adsorption of hazardous dye crystal violet from wastewater by waste materials, J. Colloid Interface Sci. 343 (2) (2010) 463–473.
- [41] S. Fateixa, H.I.S. Nogueira, T. Trindade, Surface-enhanced Raman scattering spectral imaging for the attomolar range detection of crystal violet in contaminated water, ACS Omega 3 (4) (2018) 4331–4341.
- [42] H.X. Chen, T.T. You, L. Jiang, Y.K. Gao, P.G. Yin, Creating dynamic SERS hotspots on the surface of pH-responsive microgels for direct detection of crystal violet in solution, RSC Adv. 7 (52) (2017) 32743–32748.
- [43] A.Q. Mao, X. Jin, X.L. Gu, X.Q. Wei, G.J. Yang, Rapid, green synthesis and surface-enhanced Raman scattering effect of single-crystal silver nanocubes, J. Mol. Struct. 1021 (2012) 158–161.
- [44] B. Morovvati, R. Malekfar, Surface enhanced Raman scattering of crystal violet with low concentrations using self-assembled silver and gold-silver core-shell nanoparticles, ijop 13 (2) (2019) 89–96.
- [45] E.C. Le Ru, P.G. Etchegoin, Chapter 4 SERS enhancement factors and related topics, in: E.C. Le Ru, P.G. Etchegoin (Eds.), Principles of Surface-Enhanced Raman Spectroscopy, Elsevier, Amsterdam, 2009, pp. 185–264.
- [46] Y.X. Lu, Y. Luo, Z.H. Lin, J.G. Huang, A silver-nanoparticle/cellulose-nanofiber composite as a highly effective substrate for surface-enhanced Raman spectroscopy, Beilstein J. Nanotechnol. 10 (2019) 1270–1279.
- [47] Y. Ou, L.Y. Wang, L.W. Zhu, L.S. Wan, Z.K. Xu, In-situ immobilization of silver nanoparticles on self-assembled honeycomb-patterned films enables surfaceenhanced Raman scattering (SERS) substrates, J. Phys. Chem. C 118 (21) (2014) 11478–11484.
- [48] C. Xiao, B. Mir-Simon, P. Rivera-Gil, Controlled nano-agglomerates as stabile SERS reporters for unequivocal labelling, Sci. Rep. 12 (1) (2022).
- [49] M.A. Ashraf, W.X. Peng, Y. Zare, K.Y. Rhee, Effects of size and aggregation/ agglomeration of nanoparticles on the interfacial/interphase properties and tensile strength of polymer nanocomposites, Nanoscale Res. Lett. 13 (2018).
- [50] K. Khabarov, E. Filalova, M. Nouraldeen, E. Kameneva, A. Musaev, S. Tikhonov, V. Ivanov, Effect of Au nanoparticle agglomeration on SERS signal amplification, Nanomaterials 13 (5) (2023).